ORIGINAL ARTICLE

CrossMark

Constitutive modeling of rock fractures by improved support vector regression

Nima Babanouri[1] · Hadi Fattahi[2]

Abstract

In geomechanics, constitutive models, which relate strains to stresses, have particular importance. This research concerns with developing a constitutive model for rock discontinuities. A large number of research works in this area have shed light on the most important aspects of the shear behavior of rock fractures. However, the constitutive models have been mostly developed in form of empirical functions best representing the experimental data by means of mathematical regression techniques. Thus, now there is room to upgrade the classic regression methods to the more robust modeling techniques which better capture the nonlinearity of constitutive response. In this paper, the support vector regression (SVR) enhanced with a search algorithm has been employed to construct a constitutive model for rock fractures. A series of 84 direct shear tests was conducted on concrete and plaster replicas of natural rock fractures under different levels of normal stress. The specimens had also different mechanical and morphological characteristics. The SVR constitutive model was developed based on the shear test data. The proposed model indicates significant superiority in estimating the shear strength and peak shear displacement compared to Barton–Bandis model for rock fractures.

Keywords Constitutive model · Rock fracture · Shear behavior · Support vector regression · Barton–Bandis model

Introduction

Constitutive models of geomaterials, which relate strains to stresses, are of great importance in geomechanics. Rock mass is a system composed of rock material and rock discontinuities, and hence, is described by discontinuum constitutive models. In this study, a constitutive model for rock discontinuities is developed for rock discontinuities. A large number of research works have been presented in this subject (Jaeger 1959, 1971; Patton 1966; Ladanyi and Archambault 1969; Barton 1972, 1973, 1976; Goodman 1974, 1976; Barton and Choubey 1977; Bandis et al. 1981, 1983; Barton

et al. 1985; Desai and Fishman 1987; Aydan et al. 1990; Cundall and Lemos 1990; Gens et al. 1990; Desai and Fishman 1991; Homand et al. 2001; Olsson and Barton 2001; Huang et al. 2002; Zhang and Sanderson 2002; Wang et al. 2003; Grasselli and Egger 2003; Asadollahi and Tonon 2010; Babanouri et al. 2011; Amiri Hossaini et al. 2014; Hou et al. 2016; Azinfar et al. 2016). However, there are generally two approaches used for establishing a model of rock fracture behavior: the empirical approach and theoretical approach (Jing and Stephansson 2007).

In the empirical approach, the model is developed in form of empirical functions best representing the experimental data by means of mathematical regression techniques. No constraint is considered for respecting the second law of thermodynamics in this approach. However, such models can provide agreeable results if the loading conditions and parameter ranges are suitably considered. In contrast, the theoretical approach has the thermodynamic considerations which guarantee the model obeying the second law. Nevertheless, the model parameters may not have clear physical meanings or are difficult to determine by experiments (Jing and Stephansson 2007).

✉ Nima Babanouri
   babanouri@hut.ac.ir

1   Department of Mining Engineering, Hamedan University of Technology, Hamedan, Iran

2   Department of Mining Engineering, Arak University of Technology, Arāk, Iran

A great number of the constitutive models presented for rock fractures over the years have shed light on the most important aspects of the shear behavior of rock mass. Thus, now there is room to upgrade the classic regression methods to the more robust modeling techniques which better capture the nonlinearity of constitutive response. The power of the today's computers along with the extreme complexity of shear behavior of rock joints makes it quite reasonable to suggest the application of computational intelligence for constitutive modeling.

The support vector regression (SVR) has been successfully used as a modeling tool in facing a variety of geomechanics problems (Mahdevari et al. 2014; Bagheripour et al. 2015; Elbisy 2015; Chen et al. 2016; Dai et al. 2016; Fattahi 2016; Zhu et al. 2016). However, no attempts have already been made to model the shear behavior of rock fractures using SVR.

In this paper, the support vector regression enhanced with a search algorithm has been employed to construct a constitutive model for rock fractures. A series of 84 direct shear tests was conducted on concrete and plaster replicas of natural rock fractures under different levels of normal stress. The specimens had also different mechanical and morphological characteristics. The SVR constitutive model was developed based on the experimental data. Finally, the results of the proposed model were compared to the performance of Barton–Bandis model for rock fractures.

Experimental study

Sample preparation

To keep mechanical and morphological characteristics of fractures (e.g., wall strength, and roughness) under control, a number of concrete and plaster replicas were constructed from natural rock fractures. Parent rock fractures with different values of the joint roughness coefficient (JRC) were chosen from the Gol-e-Gohar iron ore mine (Iran), and their silicon molds were prepared (Fig. 1a, b). For each of the parent surfaces, 11 digitized roughness profiles along the shear direction were considered to estimate the JRC value (Fig. 1c). Then, the average JRC values of the natural morphologies were calculated as 18.9, 12.4, 7.1, and 4.1, using the following relationship presented by Tse and Cruden (1979):

$$JRC = 32.2 + 32.47 \log Z_2, \tag{1}$$

where Z_2 is the root mean square (RMS) of the first derivative of the profile, calculated as follows (Myers 1962):

Fig. 1 Preparing silicon molds of parent rock fracture (**a**), plaster replicas with different values of JRC (**b**), location of digitized roughness profiles along the shear direction (**c**)

(a)

(b)

(c)
11 profiles
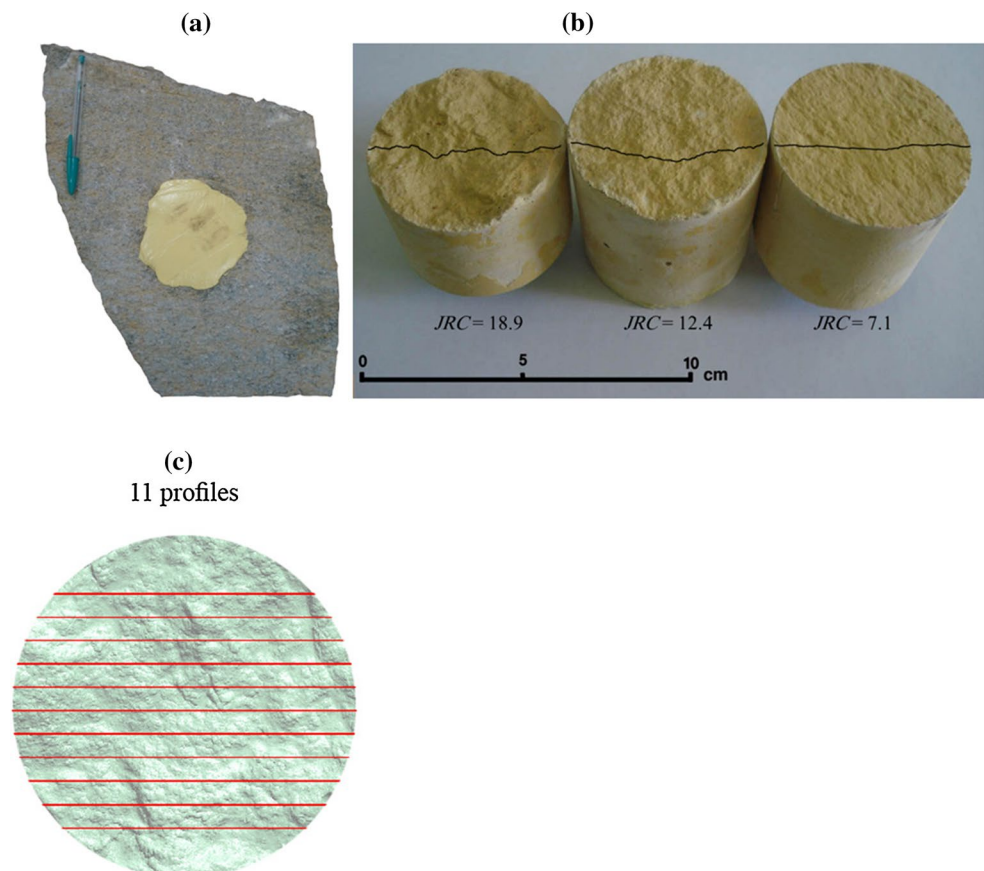
$$Z_2 = \mathrm{RMS}\left(\frac{\Delta h}{\Delta l}\right) = \left(\frac{1}{N}\sum_{i=1}^{N}\left(\frac{h_{i+1}-h_i}{l_{i+1}-l_i}\right)^2\right)^{1/2}, \qquad (2)$$

where N is the number of discrete measurements of profile coordinates (l, h).

Several superimposed pairs of each morphology were produced with different concrete and plaster materials. The specimens were cast in a cylindrical shape with a diameter of 60 mm.

To have the plaster samples cured, they were kept in a desiccator at 40 °C for 7 days. The concrete replicas were preserved in a water bath for the same time. Besides the fracture replicas, a number of intact cylindrical specimens from each material were produced. These samples were then used to measure the mechanical properties of the materials used (Fig. 2). Table 1 presents the measured mechanical parameters of the concrete and plaster materials. In this way, a series of fracture replicas with different values of roughness and mechanical properties was prepared.

Direct shear test

Direct shear testing of fracture replicas was conducted under the constant normal load (CNL) condition. The shear box was wedge type, originally pertaining to a portable shear machine (Fig. 3). Shear and normal actuators worked with two hydraulic pumps equipped with pressure adjustment and relief valves. Each actuator had a loading capacity of 50 kN, and a load cell with an accuracy of 0.04 kN measured its force. One and two LVDTs with an accuracy of 0.03 mm were in charge of measuring the shear and normal displacement, respectively. Shear load was applied to the upper part of the sample at a constant rate of about 0.5 mm/min, while the lower part was kept fixed. During the shear test, the normal displacement, normal force, shear displacement, and shear force were recorded every 0.25 s using a data acquisition system connected to a computer.

Table 1 Mechanical characteristics of materials

ID	Material	σ_c (MPa)[a]	E (GPa)[b]	ϕ_β (°)[c]
C1	Concrete	52.5	11.91	28
C2	Concrete	37.4	7.54	28
C3	Concrete	17.5	5.32	28
C4	Concrete	8.0	2.88	28
P1	Plaster	52.1	11.36	34
P2	Plaster	41.6	8.66	34
P3	Plaster	17.2	3.86	34

[a]Uniaxial compressive strength

[b]Young's modulus

[c]Basic friction angle

Figure 4 shows shear and dilation curves for a number of the performed direct shear tests. The parameters of peak shear stress (τ_p), peak shear displacement (δ_{peak}), and dilation angle (d) were extracted from the behavior curves (Fig. 5). Table 2 summarizes the specifications and results of the whole tests.

Background theories

The idea behind the proposed model is to optimize values of SVR parameters using a search algorithm. In this section, the SVR technique is explained, followed by describing the employed optimization algorithm.

Support vector regression

The support vector regression (SVR) uses the same principles as the support vector machine (SVM) for classification, with only a few minor differences. In linear SVR, a linear relationship between input data (x) and output data (y) is considered (Fig. 6a):

$$y = wx + b, \qquad (3)$$

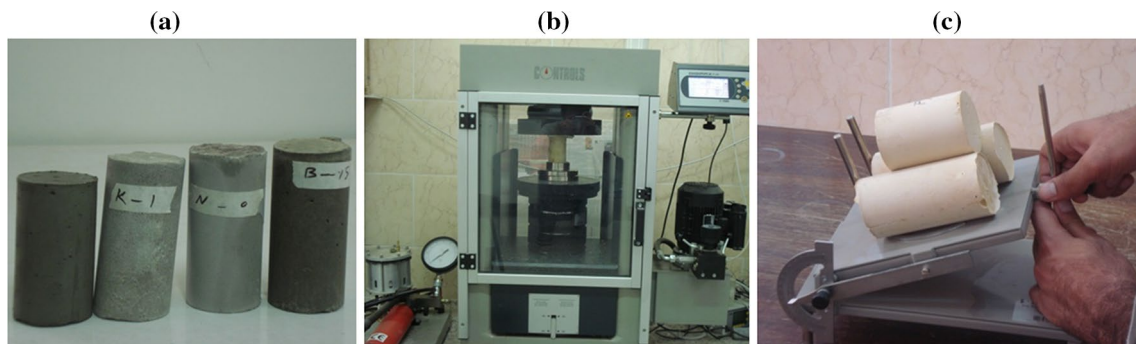The SVR method aims at minimizing the following term (Hong 2011):

Fig. 2 Measurement of mechanical properties of materials: intact cylindrical specimen (**a**), uniaxial compressive test (**b**), tilt test (**c**)
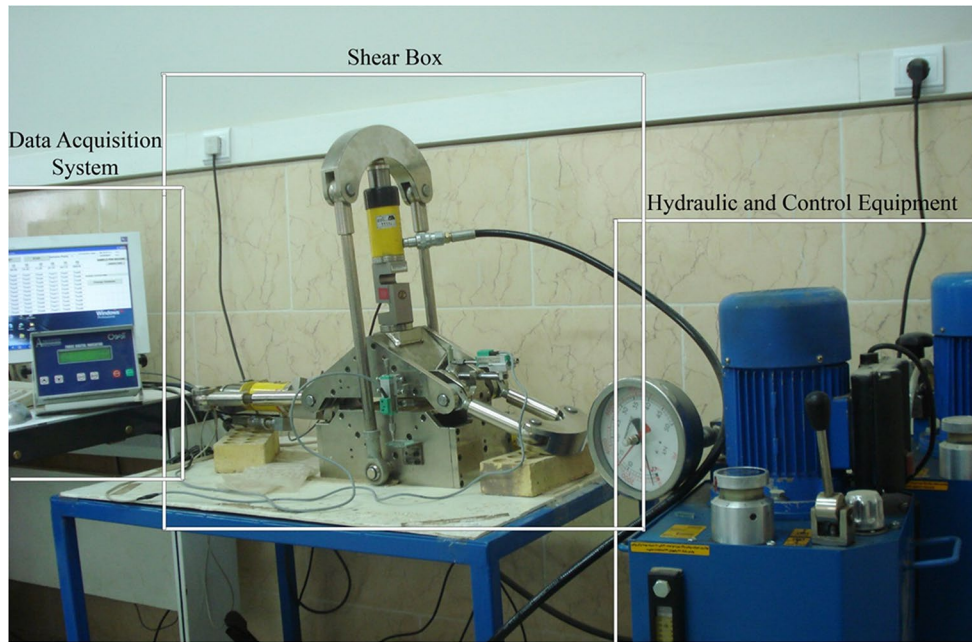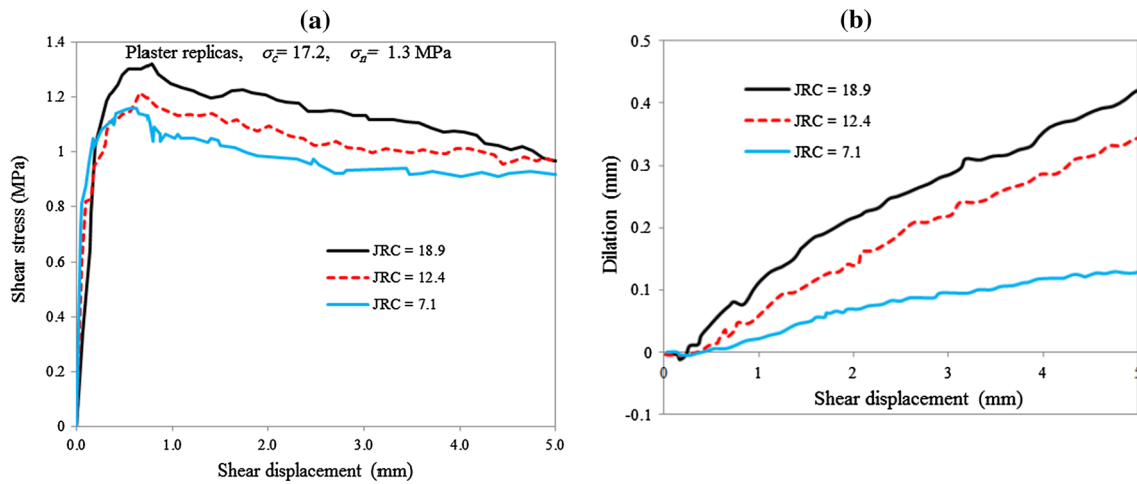
Fig. 3 Direct shear test apparatus

Fig. 4 Behavior curves for three of fracture replicas: shear curve (**a**), dilation curve (**b**)

$$\text{Minimize} \frac{1}{2}||w|| + C \sum_{i=1}^{N} \left(\xi_i^*, \xi_i \right), \tag{4}$$

with the constraints:

$$
\begin{aligned}
& y_i - wx_i - b \leq \varepsilon + \xi_i, \\
& -y_i + wx_i + b \leq \varepsilon + \xi_i^* \\
& \xi_i, \xi_i^* \geq 0.
\end{aligned}
\tag{5}
$$

The first term of Eq. (4), implying the concept of maximizing the distance of two separated training data, is used

to regularize weight sizes, to penalize large weights, and to maintain regression function flatness. The second term penalizes training errors. C is a parameter to trade off these two terms. Training errors above ε are denoted ξ_i, whereas training errors below $-\varepsilon$ are denoted as ξ_i^* (Fig. 6a). After the quadratic optimization problem with inequality constraints is solved, the vector w is obtained in terms of two Lagrangian multipliers.

In nonlinear SVR, which is used in this study, the kernel functions transform the data into a higher-dimensional feature space to make it possible to perform the linear separation (Fig. 6b). The value of the kernel equals the inner
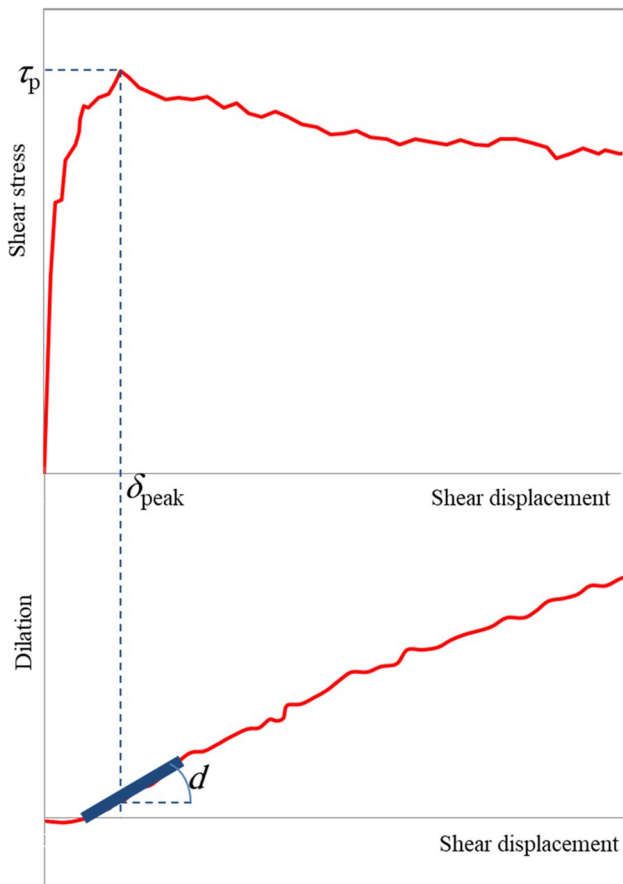
Fig. 5 Extraction of shear behavior parameters from shear and dilation curves

product of two vectors, x_i and x_j, in the feature space $\varphi(x_i)$ and $\varphi(x_j)$ as follows (Hong 2011):

$$K\left(x_i, x_j\right) = \varphi(x_i)\varphi(x_j). \tag{6}$$

There are several types of kernel function, but in this study, we used a most common and powerful of them. This kernel function is called radial basis kernel function (RBF) defined as below:

$$K\left(x_i, x_j\right) = \exp\left(-\frac{\left\|x_i - x_j\right\|}{2\sigma^2}\right). \tag{7}$$

C, σ, and ε are three main parameters of the SVR that are optimized in training state.

BBO search algorithm

The biogeography-based optimization (BBO) is similar to other population-based optimization techniques where population of candidate solutions $\{x\}$ is represented as a vector

of real numbers (Simon 2008). A pseudo-code for the BBO algorithm used in this study is given in Fig. 7. Each element in the solution array is considered as one suitability independent variable (SIV). Fitness of each set of candidate solution is evaluated using a fitness function. The probability of emigration, μ, for each solution is calculated proportionally to its fitness, and the probability of immigration is calculated as $\lambda = 1 - \mu$.

The emigration and immigration probabilities of each solution are used to probabilistically share information between habitats. Using habitat modification probability, each solution is modified based on other solutions. Immigration probability of each solution is used to probabilistically decide whether or not to modify each SIV in that solution. After selecting SIV for modification, emigration probabilities of other solutions are used to probabilistically select which solutions among the population set will migrate. In order to prevent the best solutions from being corrupted by the immigration process, few elite solutions are kept in the BBO algorithm. Like most other evolutionary algorithms, BBO includes mutation of a percent of solutions to increase diversity among the populations. Here, mutation of a selected solution is performed simply by replacing it with randomly generated new solution set. Other than this, any other mutation scheme that has been implemented for genetic algorithm can also be implemented for BBO (Roy et al. 2010).

SVR-BBO constitutive modeling of rock fractures

Inputs and output data

The inputs of the model were once considered to be JRC, joint wall compressive strength (JCS) which is equal to uniaxial compressive strength (σ_c), Young's modulus (E), normal stress (σ_n), and basic friction angle (ϕ_b), while the outputs were τ_p, δ_{peak}, and d. Although the basic friction angle of rock fractures has generally a limited range, this parameter plays an important role and cannot be ignored in constitutive modeling of rock joints. The deformability of rock fracture asperities (represented by the Young's modulus of rock materials in this study) influences the contact area during shearing and consequently affects the shear behavior of fractures. In fact, the incorporation of the Young's modulus is a step forward in constitutive modeling of rock fractures. However, since the Young's modulus of rock fracture asperities may not always be measured, the model was construted another time excluding the parameter of E from the inputs. The dataset was randomly divided into two sets of training and testing with 67 and 17 samples, respectively.

Table 2 Specifications of direct shear tests along with measured values of rock joint shear strength

Test no.	Mat. ID	JRC	σ_n (MPa)	τ_p (MPa)	δ_{peak} (mm)	d (°)
1	C1	18.9	0.57	0.67	0.42	15.9
2	C1	18.9	1.3	1.31	0.39	13.7
3	C1	18.9	2	1.67	0.35	11.3
4	C1	18.9	2.5	2.54	0.29	10.7
5	C1	4.1	0.57	0.46	0.87	3.9
6	C1	7.1	0.57	0.45	0.52	4.4
7	C1	12.4	0.57	0.45	0.48	10.6
8	C1	12.4	1.3	1.24	0.45	10.1
9	C1	7.1	1.3	1.07	0.50	3.4
10	C1	4.1	1.3	1.00	0.75	4.2
11	C1	4.1	2	0.94	0.64	0.0
12	C1	12.4	2	1.46	0.44	7.8
13	C1	7.1	2	1.05	0.48	3.6
14	C1	12.4	2.5	2.09	0.40	5.7
15	C1	4.1	2.5	1.45	0.60	0.0
16	C1	7.1	2.5	1.82	0.44	3.3
17	C3	18.9	0.57	0.68	0.61	18.2
18	C3	4.1	0.57	0.48	0.82	3.5
19	C3	7.1	0.57	0.42	0.99	4.9
20	C3	12.4	0.57	0.49	0.74	8.8
21	C3	18.9	1.3	1.03	0.48	10.0
22	C3	4.1	1.3	0.72	0.87	0.0
23	C3	12.4	1.3	0.94	0.69	7.4
24	C3	7.1	1.3	0.77	0.75	3.8
25	C3	7.1	2	1.23	0.46	2.5
26	C3	18.9	2	1.67	0.37	8.5
27	C3	12.4	2	1.37	0.40	5.7
28	C3	4.1	2	1.22	0.52	0.0
29	C2	7.1	0.57	0.40	0.70	4.9
30	C2	7.1	1.3	0.82	0.65	3.5
31	C2	18.9	0.57	0.75	0.52	15.1
32	C2	12.4	0.57	0.50	0.63	9.5
33	C2	7.1	2	1.30	0.52	2.8
34	C2	18.9	1.3	1.34	0.50	11.3
35	C2	12.4	1.3	0.92	0.60	7.6
36	C2	18.9	2	1.82	0.46	9.9
37	C2	12.4	2	1.08	0.52	6.0
38	C2	18.9	2.5	2.04	0.40	8.5
39	C2	12.4	2.5	1.44	0.40	5.0
40	C4	18.9	0.57	0.57	1.11	8.7
41	C4	12.4	0.57	0.46	0.87	5.6
42	C4	7.1	0.57	0.40	0.35	2.5
43	C4	7.1	2	1.13	0.47	0.6
44	C4	18.9	1.3	1.08	0.75	6.8
45	C4	18.9	2	1.30	0.72	4.8
46	C4	12.4	1.3	0.90	0.64	4.9
47	C4	12.4	2	1.27	0.58	3.5
48	C3	7.1	2.5	1.08	0.33	0.0
49	C3	12.4	2.5	1.42	0.40	4.3
50	C3	18.9	2.5	1.69	0.40	4.3
51	P3	4.1	0.57	0.51	0.75	2.3

Table 2 (continued)

| Test no.	Mat. ID	JRC	σ_n (MPa)	τ_p (MPa)	δ_{peak} (mm)	d (°)
52	P3	7.1	0.57	0.57	0.87	3.9
53	P3	12.4	0.57	0.71	0.93	8.9
54	P3	18.9	0.57	0.74	0.98	11.8
55	P3	4.1	1.3	1.05	0.62	0.0
56	P3	7.1	1.3	1.16	0.64	2.7
57	P3	12.4	1.3	1.22	0.70	6.9
58	P3	18.9	1.3	1.32	0.80	9.2
59	P3	4.1	2	1.61	0.60	0.0
60	P3	7.1	2	1.67	0.64	2.2
61	P3	12.4	2	1.85	0.70	4.9
62	P2	4.1	0.57	0.37	0.75	3.4
63	P2	7.1	0.57	0.46	0.70	4.1
64	P2	18.9	0.57	0.62	0.58	13.1
65	P2	4.1	1.3	0.84	0.64	2.7
66	P2	7.1	1.3	0.87	0.64	3.1
67	P2	12.4	1.3	1.27	0.60	6.7
68	P2	18.9	1.3	1.33	0.52	10.4
69	P2	4.1	2	1.57	0.57	2.5
70	P2	7.1	2	1.64	0.55	2.6
71	P2	12.4	2	1.83	0.46	7.4
72	P2	18.9	2	2.29	0.40	9.2
73	P1	4.1	0.57	0.39	0.52	3.9
74	P1	7.1	0.57	0.39	0.81	4.2
75	P1	12.4	0.57	0.58	0.64	10.6
76	P1	18.9	0.57	0.58	0.58	14.5
77	P1	4.1	1.3	0.64	0.55	3.1
78	P1	7.1	1.3	0.90	0.50	3.4
79	P1	12.4	1.3	1.12	0.46	9.9
80	P1	18.9	1.3	1.10	0.34	10.8
81	P1	4.1	2	1.12	0.52	0.6
82	P1	7.1	2	1.38	0.50	3.4
83	P1	12.4	2	1.61	0.44	7.8
84	P1	18.9	2	2.06	0.50	9.6
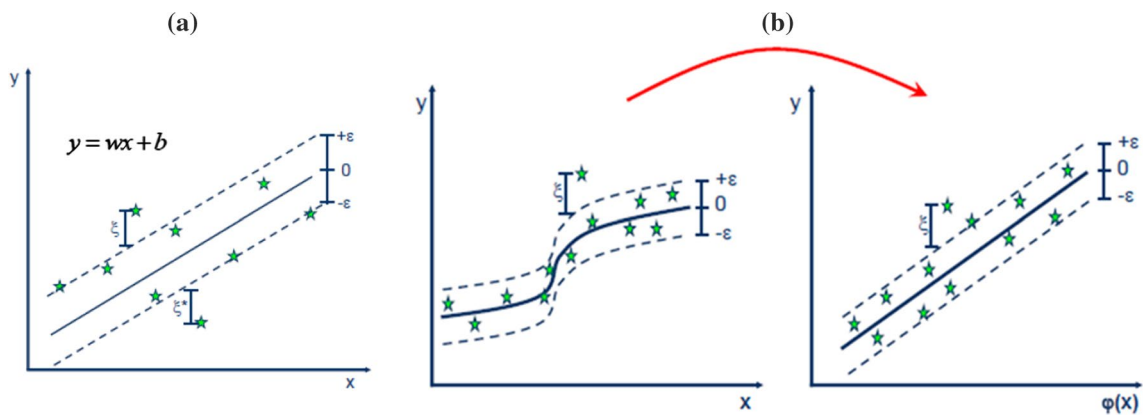
Fig. 6 Support vector regression: linear SVR (**a**), nonlinear SVR (**b**) (www.saedsayad.com 2018)

Fig. 7 Pseudo-code for BBO algorithm used in this study (after Wikipedia Contributors 2017)

```
- Initialize a population of N candidate solutions {xk} of an n-dimensional function
- While not exceeding the maximum number of iterations
      For each xk, set emigration probability μk proportional to fitness of xk, with μk ∈ [0,1]
      For each xk, set immigration probability λk = 1- μk
      {zk} ← {xk}
      For each individual zk (k = 1,..., N)
                  For each independent variable index s ∈ [1,n]
                        Use λk to probabilistically decide whether to immigrate to zk
                        If immigrating then
                              Use {μi} to probabilistically select the emigrating individual xj
                              zk(s) ← xj(s)
                        End if
                        Next independent variable index: s ← s+1
                  Probabilistically mutate zk with the percentage of m
      Next individual: k ← k+1
      {xk} ← {zk}
- Next iteration
```

Hybrid SVR-BBO model

The generalization capability of SVR is extremely dependent upon its learning parameters, i.e., the regularization parameter $C \in \left[2^{-5}, 2^{15}\right]$, the RBF kernel parameter $\sigma \in \left[2^{-5}, 2^{3}\right]$, and the error margin $\varepsilon \in [0.01, 0.6]$, to be set correctly. Finding the best combination of the hyper-parameters is often troublesome due to the highly nonlinear space of the model performance with respect to these parameters. In this paper, a BBO algorithm was adopted in order to improve the learning procedure of SVR through finding optimal values of its parameters. Figure 8 introduces the flowchart of the hybrid SVR-BBO model used in this study.

Preprocessing of data

In data-driven system modeling methods, some preprocessing steps are commonly implemented prior to any calculations in order to eliminate any outliers, missing values, or bad data. This step ensures that the raw data retrieved from the database are perfectly suitable for modeling. In order for softening the training procedure and improving the accuracy of prediction, all data samples are normalized to adapt to the interval [-1, 1] according to the following linear mapping function:

$$x_M = 2\left(\frac{x - x_{\min}}{x_{\max} - x_{\min}}\right) - 1, \tag{8}$$

where x is the original value from the dataset, x_M is the mapped value, and $x_{\min}$ ($x_{\max}$) denotes the minimum (maximum) raw input values, respectively.

Results

Parameter regularizations for running the optimization models were obtained by trial-and-error procedure (Tables 3, 4, 5). The values of the adjusted parameters $\{C, \sigma, \varepsilon\}$ producing maximal accuracy were considered to be the most appropriate values of the parameters. The best parameter values obtained by each model are presented in Tables 6, 7, 8. The optimal values were then used to retrain the SVR models.

Figures 9, 10, and 11 show the performance of the constitutive model with E for the different shear behavior parameters in the training and testing stages. As can be seen, the model has provided agreeable results in both the training and testing phases. The performance of the model in the training phase shows its capability to capture the input–output patterns, and the performance at the testing phase shows the power of the model in facing unseen data.

Discussion

In order to better evaluate the proposed model, it was compared to the well-known Barton–Bandis (BB) constitutive model for rock fractures. The BB model is a series of empirical relationships developed to describe deformation and strength of rock fractures (Barton 1972, 1973, 1976; Bandis et al. 1981, 1983; Barton et al. 1985). The shear strength, peak shear displacement, and dilation angle are, respectively, estimated as below (Barton 1973, 1976; Barton and Choubey 1977; Barton et al. 1985):

$$\tau_p = \sigma_n \tan\left[\varphi_b + \text{JRC} \cdot \log_{10}\left(\frac{\text{JCS}}{\sigma_n}\right)\right], \tag{9}$$
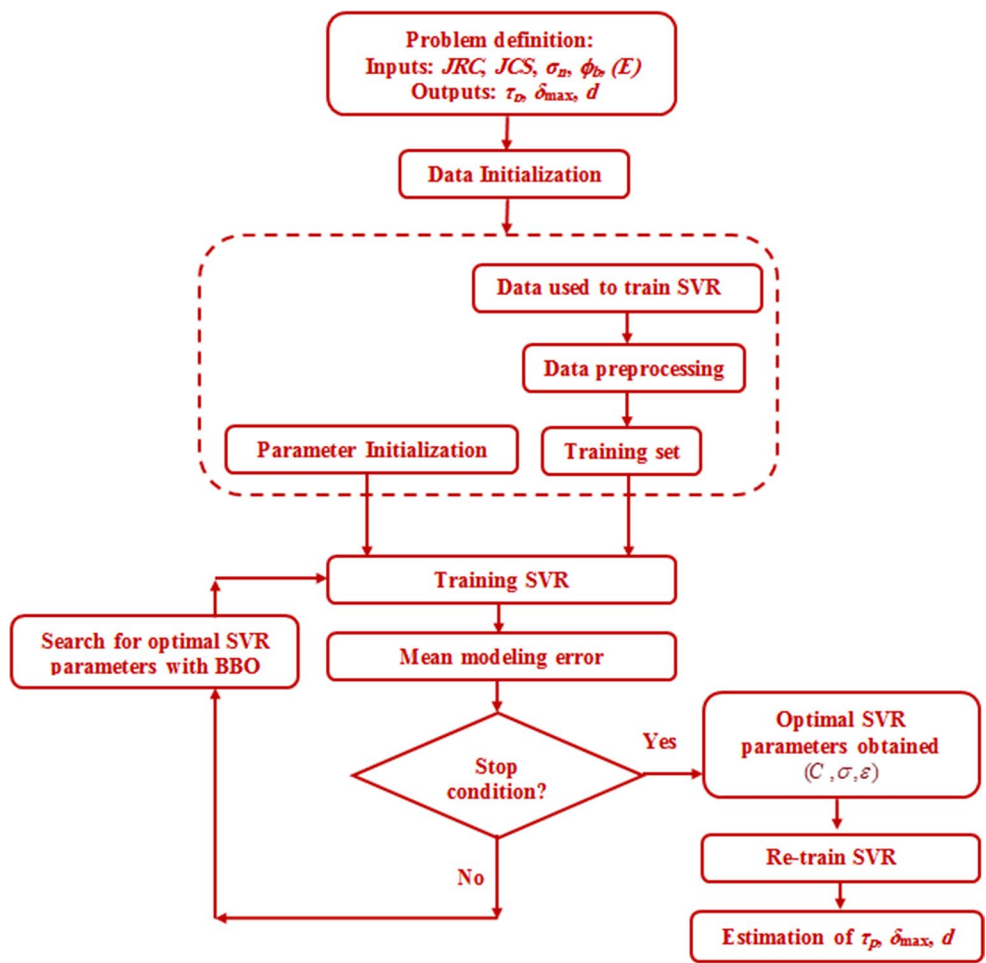
Fig. 8 Process of optimizing the SVR parameters by BBO

Table 3 Regulated parameters of BBO algorithm for estimation of shear strength

Definition	Value
Number of habitats (population size)	50
Highest number of repeat algorithm steps	600
Percentage of mutation	0.11
Percentage of old population that is directly transferred to the new population	0.2

Table 4 Regulated parameters of BBO algorithm for estimation of peak shear displacement

Definition	Value
Number of habitats (population size)	45
Highest number of repeat algorithm steps	700
Percentage of mutation	0.1
Percentage of old population that is directly transferred to the new population	0.2

Table 5 Regulated parameters of BBO algorithm for estimation of dilation angle

Definition	Value
Number of habitats (population size)	50
Highest number of repeat algorithm steps	650
Percentage of mutation	0.09
Percentage of old population that is directly transferred to the new population	0.2

Table 6 Optimal parameters of SVR obtained by BBO for estimation of shear strength

Optimal value of σ parameter	Optimal value of C parameter	Optimal value of ε parameter
3.3529	2714	0.279

$$\delta_{\text{peak}} = \frac{L_n}{500} \left(\frac{\text{JRC}}{L_n} \right)^{0.33}, \tag{10}$$

Optimal value of σ parameter	Optimal value of C parameter	Optimal value of ε parameter
3.3539	2824	0.286

Optimal value of σ parameter	Optimal value of C parameter	Optimal value of ε parameter
1.3585	2722	0.151

$$d = 0.5 \text{JRC}_{\text{mob}} \cdot \log \left(\frac{\text{JCS}_n}{\sigma_n} \right), \qquad (11)$$

where L_n is the rock fracture length which is given in meters as well is δ_{peak}.

The BB model does not incorporate Young's modulus. Therefore, it was compared to the SVR model developed without E. Figures 12, 13, and 14 show the performance of the BB model in comparison with the proposed model for predicting the different parameters. As can be seen, the values of root mean square error (RMSE) indicate significant superiority of the developed model in estimating the shear strength and peak shear displacement, compared to the BB model. Especially, the BB model is unable to provide a good estimation of δ_{peak} and to
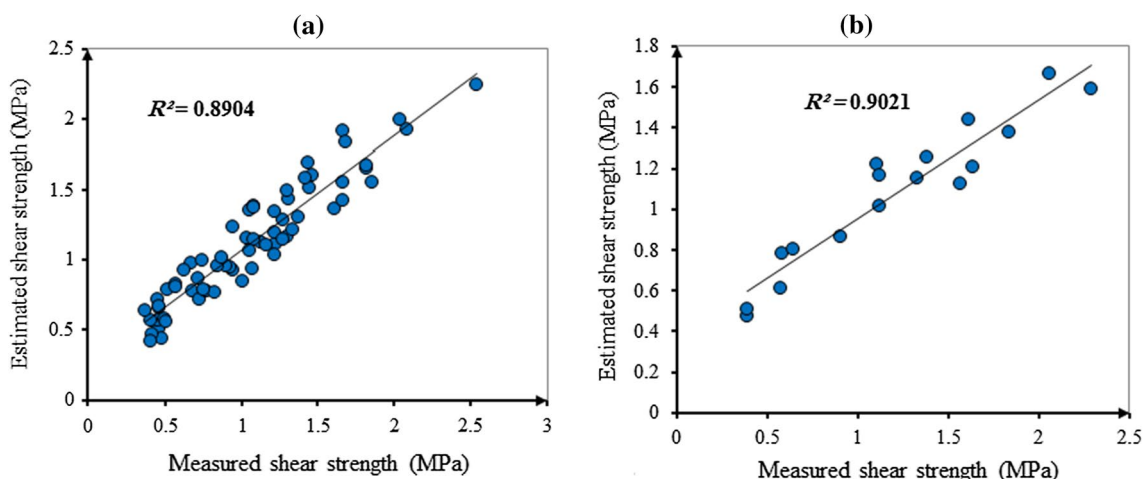
Fig. 9 Performance of SVR constitutive model for shear strength in training stage (**a**) and testing stage (**b**)
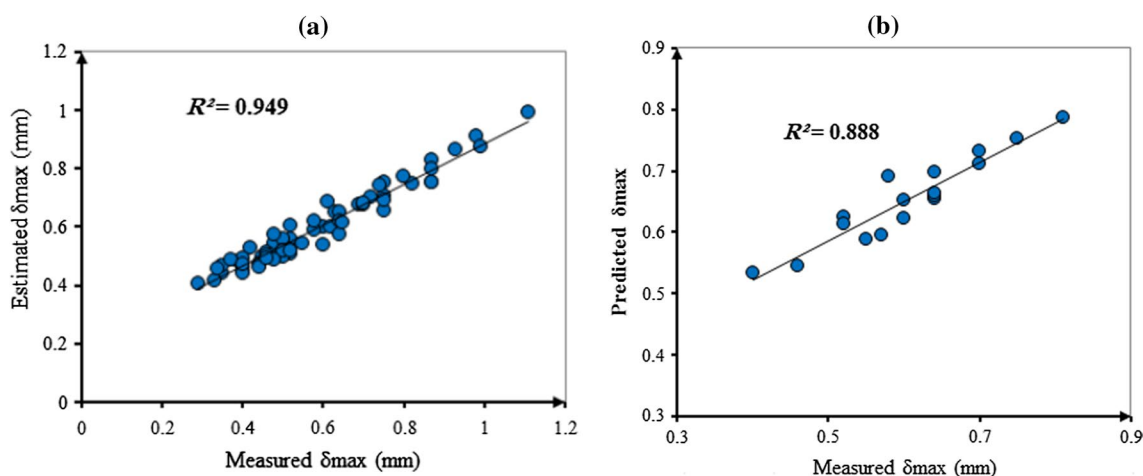

Fig. 10 Performance of SVR constitutive model for peak shear displacement in training stage (**a**) and testing stage (**b**)
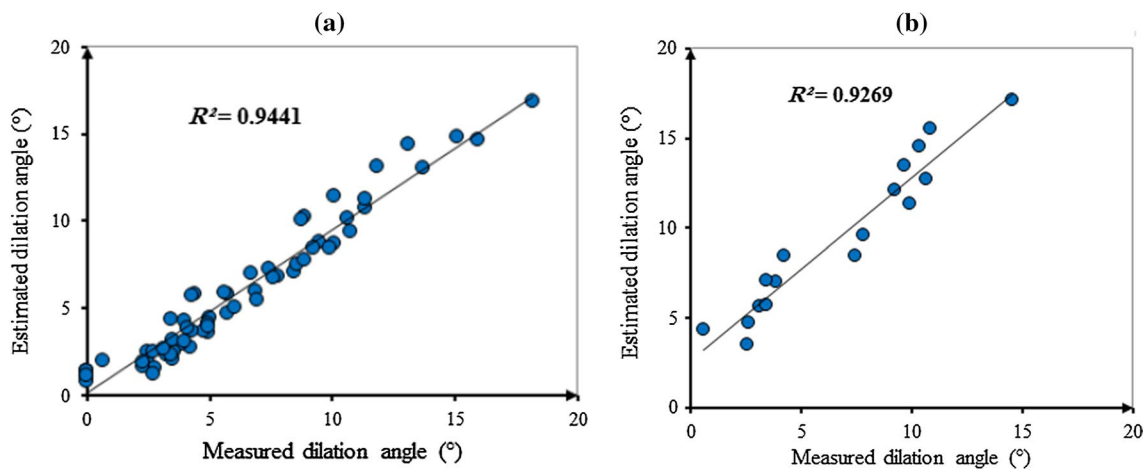
Fig. 11 Performance of SVR constitutive model for dilation angle in training stage (**a**) and testing stage (**b**)

Fig. 12 Performance of BB model in comparison with proposed model for shear strength
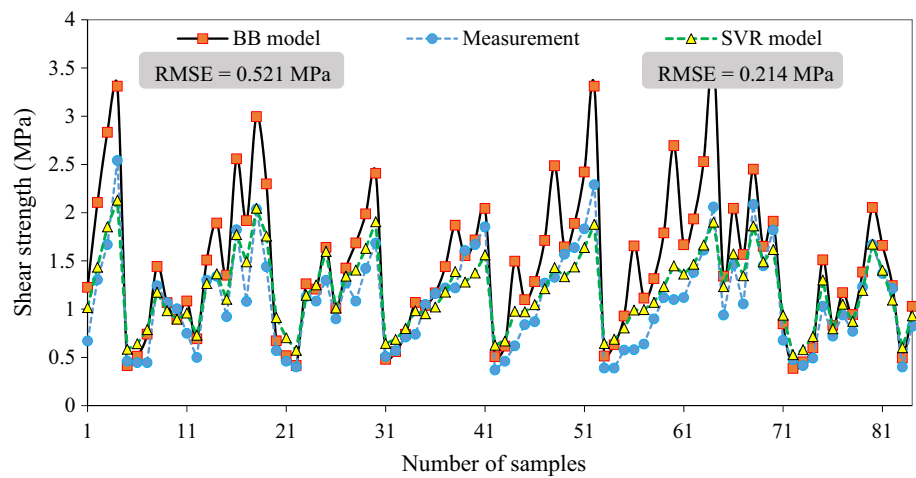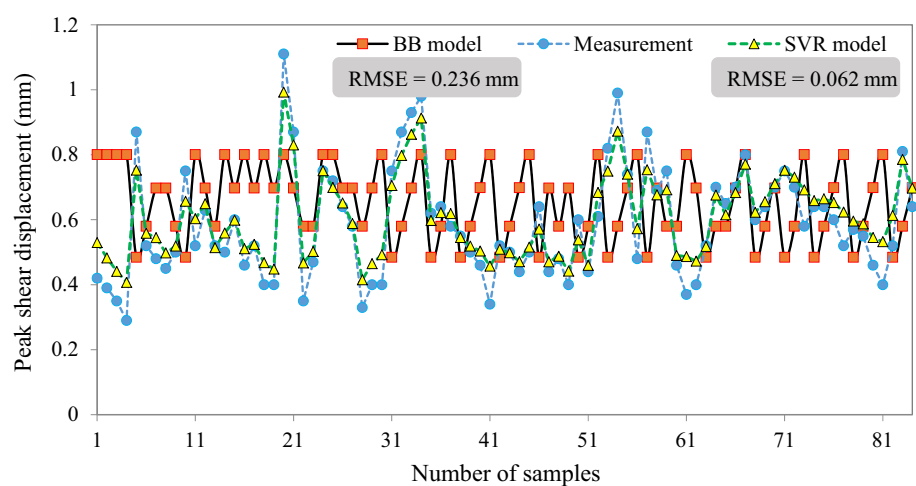

Fig. 13 Performance of BB model in comparison with proposed model for peak shear displacement

capture the nonlinearity of the problem. However, in case of the dilation angle, both the models demonstrate the same performance.

The scale effect is beyond the scope of this research; therefore, the obtained results cannot be directly extended to large scale behavior. However, since the developed model

Fig. 14 Performance of BB model in comparison with proposed model for dilation angle
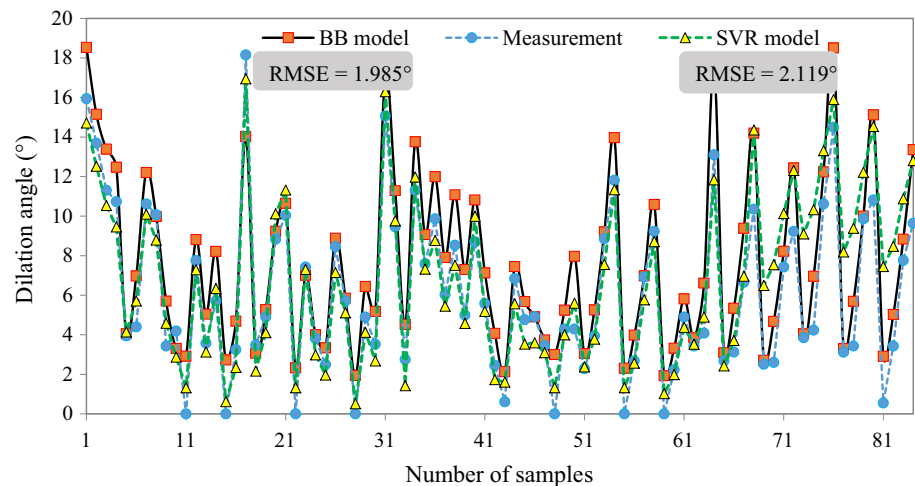
is a JRC–JCS model, it can benefit from the relationships presented for upscaling of JRC and JCS (Bandis et al. 1981; Barton et al. 1985) to consider the effect of scale.

Conclusions

This research developed a constitutive model for rock discontinuities in which the support vector regression was used instead of classic techniques of regression. The model was established based on the results of a systematic set of 84 direct shear tests. The efficiency of SVR in capturing the nonlinear behavior of rock fractures was enhanced through its combination with a search algorithm.

The performance of the developed constitutive model for estimating τ_p, δ_{peak}, and d based on JRC, JCS, (E), σ_n, and ϕ_b was promising in spite of high nonlinearity of shear behavior of rock fractures. The model proved its capability to capture the input–output patterns, and its power when facing unseen data.

On the other hand, comparative investigations revealed that the Barton–Bandis model had a good performance only for estimating the dilation angle and was incapable of modeling the more complicated parameters such as peak shear displacement. Hence, the application of computational intelligence for constitutive modeling is recommended in line with increasing the power of computers.

References

Amiri Hossaini K, Babanouri N, Karimi Nasab S (2014) The influence of asperity deformability on the mechanical behavior of rock joints. Int J Rock Mech Min Sci 70:154–161. https://doi.org/10.1016/j.ijrmms.2014.04.009

Asadollahi P, Tonon F (2010) Constitutive model for rock fractures: revisiting Barton's empirical model. Eng Geol 113:11–32

Aydan O, Ichikawa Y, Ebisu S et al (1990) Studies on interfaces and discontinuities and an incremental elasto-plastic constitutive law. In: Proceedings of international conference on rock joints, ISRM, pp 595–601

Azinfar M, Ghazvinian A, Nejati H (2016) Assessment of scale effect on 3D roughness parameters of fracture surfaces. Eur J Environ Civ Eng. https://doi.org/10.1080/19648189.2016.1262286

Babanouri N, Karimi Nasab S, Baghbanan A, Mohamadi HR (2011) Over-consolidation effect on shear behavior of rock joints. Int J Rock Mech Min Sci 48:1283–1291. https://doi.org/10.1016/j.ijrmms.2011.09.010

Bagheripour P, Gholami A, Asoodeh M, Vaezzadeh-Asadi M (2015) Support vector regression based determination of shear wave velocity. J Petrol Sci Eng 125:95–99. https://doi.org/10.1016/j.petrol.2014.11.025

Bandis S, Lumsden A, Barton NR (1981) Experimental studies of scale effects on the shear behaviour of rock joints. Int J Rock Mech Min Sci Geomech Abstr 18:1–21

Bandis SC, Lumsden AC, Barton NR (1983) Fundamentals of rock joint deformation. Int J Rock Mech Min Sci Geomech Abstr 20:249–268. https://doi.org/10.1016/0148-9062(83)90595-8

Barton NR (1972) A model study of rock-joint deformation. Int J Rock Mech Min Sci Geomech Abstr 9(5):579–582

Barton N (1973) Review of a new shear-strength criterion for rock joints. Eng Geol 7:287–332. https://doi.org/10.1016/0013-7952(73)90013-6

Barton N (1976) The shear strength of rock and rock joints. Int J Rock Mech Min Sci Geomech Abstr 13:255–279. https://doi.org/10.1016/0148-9062(76)90003-6

Barton N, Choubey V (1977) The shear strength of rock joints in theory and practice. Rock Mech 10:1–54. https://doi.org/10.1007/BF01261801

Barton N, Bandis S, Bakhtar K (1985) Strength, deformation and conductivity coupling of rock joints. Int J Rock Mech Min Sci Geomech Abstr 22(3):121–140

Chen M, Lu W, Xin X et al (2016) Critical geometric parameters of slope and their sensitivity analysis: a case study in Jilin, Northeast China. Environ Earth Sci 75:832. https://doi.org/10.1007/s12665-016-5623-4

Cundall PA, Lemos JV (1990) Numerical simulation of fault instabilities with a continuously-yielding joint model. In: Proceedings of rockbursts and seismicity in mines. Balkema, Rotterdam, pp 147–152

Dai L, Mao J, Wang Y et al (2016) Optimal operation of the Three Gorges Reservoir subject to the ecological water level of Dongting Lake. Environ Earth Sci 75:1111. https://doi.org/10.1007/s12665-016-5911-z

Desai CS, Fishman KL (1987) Constitutive models for rocks and discontinuities (joints). In: The 28th US symposium on rock mechanics (USRMS). American Rock Mechanics Association

Desai CS, Fishman KL (1991) Plasticity-based constitutive model with associated testing for joints. Int J Rock Mech Min Sci Geomech Abstr 28(1):15–26

Elbisy MS (2015) Support Vector Machine and regression analysis to predict the field hydraulic conductivity of sandy soil. KSCE J Civ Eng 19:2307–2316. https://doi.org/10.1007/s12205-015-0210-x

Fattahi H (2016) Application of improved support vector regression model for prediction of deformation modulus of a rock mass. Eng Comput 32:567–580. https://doi.org/10.1007/s00366-016-0433-6

Gens A, Carol I, Alonso EE (1990) A constitutive model for rock joints formulation and numerical implementation. Comput Geotech 9:3–20

Goodman RE (1974) The mechanical properties of joints. In: Proceedings of the third international congress international society of rock mechanics Denver, Colorado. National Academy of Sciences, Washington, DC, pp 127–140

Goodman RE (1976) Methods of geological engineering in discontinuous rocks. West Information Publishing Group

Grasselli G, Egger P (2003) Constitutive law for the shear strength of rock joints based on three-dimensional surface parameters. Int J Rock Mech Min Sci 40:25–40. https://doi.org/10.1016/S1365-1609(02)00101-6

Homand F, Belem T, Souley M (2001) Friction and degradation of rock joint surfaces under shear loads. Int J Numer Anal Methods Geomech 25:973–999

Hong W-C (2011) Electric load forecasting by seasonal recurrent SVR (support vector regression) with chaotic artificial bee colony algorithm. Energy 36:5568–5578

Hou D, Rong G, Yang J et al (2016) A new shear strength criterion of rock joints based on cyclic shear experiment. Eur J Environ Civ Eng 20:180–198. https://doi.org/10.1080/19648189.2015.1021383

Huang TH, Chang CS, Chao CY (2002) Experimental and mathematical modeling for fracture of rock joint with regular asperities. Eng Fract Mech 69:1977–1996

Jaeger JC (1959) The frictional properties of joints in rock. Pure Appl Geophys 43:148–158

Jaeger JC (1971) Friction of rocks and stability of rock slopes. Geotechnique 21:97–134

Jing L, Stephansson O (2007) Constitutive models of rock fractures and rock masses—the basics. In: Jing L, Stephansson O (eds) Fundamentals of discrete element methods for rock engineering theory and applications. Elsevier, Amsterdam, pp 47–109

Ladanyi B, Archambault G (1969) Simulation of shear behavior of jointed rock mass. In: 11th U.S. symposium on rock mechanics: theory and practice. Berkeley, pp 105–125

Mahdevari S, Shahriar K, Yagiz S, Akbarpour Shirazi M (2014) A support vector regression model for predicting tunnel boring machine penetration rates. Int J Rock Mech Min Sci 72:214–229. https://doi.org/10.1016/j.ijrmms.2014.09.012

Myers NO (1962) Characterization of surface roughness. Wear 5:182–189

Olsson R, Barton N (2001) An improved model for hydromechanical coupling during shearing of rock joints. Int J Rock Mech Min Sci 38:317–329

Patton FD (1966) Multiple modes of shear failure in rock. In: Proceedings of the 1st international congress on rock mechanics. International Society for Rock Mechanics, Lisbon, pp 509–513

Roy PK, Ghoshal SP, Thakur SS (2010) Biogeography based optimization for multi-constraint optimal power flow with emission and non-smooth cost function. Expert Syst Appl 37:8221–8228

Simon D (2008) Biogeography-based optimization. IEEE Trans Evol Comput 12:702–713

Tse R, Cruden DM (1979) Estimating joint roughness coefficients. Int J Rock Mech Min Sci Geomech Abstr 16:303–307. https://doi.org/10.1016/0148-9062(79)90241-9

Wang JG, Ichikawa Y, Leung CF (2003) A constitutive model for rock interfaces and joints. Int J Rock Mech Min Sci 40:41–53

Wikipedia contributors (2017) Biogeography-based optimization. In: Wikipedia, the free encyclopedia. https://en.wikipedia.org/w/index.php?title=Biogeography-based_optimization&oldid=814002840. Accessed 18 Jan 2018

www.saedsayad.com (2018) Support vector regression. http://www.saedsayad.com/support_vector_machine_reg.htm. Accessed 18 Jan 2018

Zhang X, Sanderson DJ (2002) Numerical modelling and analysis of fluid flow and deformation of fractured rock masses. Elsevier, Amsterdam

Zhu S, Zhou J, Ye L, Meng C (2016) Streamflow estimation by support vector machine coupled with different methods of time series decomposition in the upper reaches of Yangtze River, China. Environ Earth Sci 75:531. https://doi.org/10.1007/s12665-016-5337-7